electronics

MDPI

Article

Power Hardware-in-the-Loop Smart Inverter Testing with Distributed Energy Resource Management Systems

Hao Chang * and Luigi Vanfretti *

Electrical, Computer, and Systems Engineering (ECSE), Rensselaer Polytechnic Institute, Troy, NY 12180, USA
* Correspondence: changh7@rpi.edu (H.C.); vanfrl@rpi.edu (L.V.)

Abstract: The increasing integration of grid-connected photovoltaic (PV) inverters and inverter-based resource (IBR) systems into the power grid emphasizes the critical need for standardized procedures to ensure their reliability and effective grid support functions. This research is driven by the gap in standardized testing methodologies for smart inverters, which are pivotal for the stability and quality of power in distributed energy systems. We used a Power Hardware-in-the-Loop (PHIL) laboratory setup to conduct a comprehensive analysis of smart inverters within a simulated real-world grid environment. Our approach integrates a Distributed Energy Resource Management System (DERMS) with PHIL testing to evaluate the smart inverter's performance across various operational modes. The detailed test protocols mimic real-world grid conditions, enabling the examination of the inverter's dynamic response to grid disturbances, control strategies, and communication protocols. The primary aim of this study is to rigorously test and validate the primary functions of smart inverters, focusing on their impact on overall grid stability and power quality management. This includes advanced features like Volt–VAR, Volt–Watt, dynamic power factor control, and the seamless integration of smart inverters into DERMSs and Advanced Distribution Management Systems (ADMSs). Furthermore, we aim to bridge the current gap in standardized testing procedures, contributing to the establishment of robust standards and operating protocols for smart inverter integration into the grid.

Keywords: PV inverter; power hardware-in-the-loop; real-time simulation; DERM; IEEE 1547

Citation: Chang, H.; Vanfretti, L. Power Hardware-in-the-Loop Smart Inverter Testing with Distributed Energy Resource Management Systems. *Electronics* **2024**, *13*, 1866. https://doi.org/10.3390/electronics13101866

Academic Editors: Ahmed Abu-Siada, Irfan Ahmad Khan and Francisco Javier Ruiz-Rodríguez

Received: 16 January 2024
Revised: 28 April 2024
Accepted: 5 May 2024
Published: 10 May 2024

1. Introduction

The integration of grid-connected photovoltaic (PV) inverters and other power electronics in inverter-based resource (IBR) systems is becoming increasingly important. This integration is contingent upon meeting specific criteria outlined in various standards [1] and grid codes [2]. Despite significant progress in evaluating IBR technologies for grid integration, conventional simulation methods, such as those used in interconnection studies [3], often fall short of fully capturing their dynamic performance.

A thorough evaluation of the cyber-physical performance of IBRs is generally accomplished through hardware-only tests. However, these tests are expensive and time-intensive, and carry the risk of damaging the test equipment. An alternative approach to examine the "cyber" characteristics, such as control systems and communication protocols of new technologies [4], is the implementation of real-time simulation with Controller Hardware-in-the-Loop (CHIL, HIL) [5]. Notably, CHIL allows for conducting destructive tests to examine internal protections without harming the test equipment [6]. Complementing CHIL and HIL, Power Hardware-in-the-Loop (PHIL) testing [7] offers a cost-effective and efficient method to evaluate the performance of power electronics systems in non-destructive, real-world conditions.

Recently, PHIL testing for power electronics systems, including smart inverters, has garnered increasing interest. Various studies have underscored the advantages of PHIL over traditional testing methods, such as purely simulated or hardware-based approaches.

For instance, ref. [8] introduced a PHIL testbed for grid-connected PV inverters, highlighting its superior accuracy and reliability compared to purely simulated tests. Additionally, the research in [9] explored the stability of a 100 W inverter's PHIL testing environment.

This paper aims to enhance the testing and development of power electronics systems, thereby facilitating more dependable, efficient, and safe utilization of smart inverters in renewable energy applications. Here, we focus on an inverter with a power rating of 150 kW1. Our experimental setup tests the inverter under conditions that closely mimic real-world scenarios, albeit at a reduced capacity for the test specimen. The laboratory facility has been designed to evaluate both cyber and physical aspects, although this paper predominantly discusses electrical performance aspects; a subsequent companion paper will address data communications and control.

The main contributions of this work are to provide a Power-Hardware-in-the-Loop-based laboratory design that considers both the electrical and the communications systems required for testing smart inverter functionalities including a DERMS, as well as examples of the verification experiments that were conducted on a real-world smart inverter.

The structure of this paper is as follows. In Section 2, relevant literature is concisely summarized and contrasted with the authors' work. In Section 3 the laboratory's design is outlined, while Section 4 details the individual components/sub-systems of the testbed. Section 5 presents a typical test application using this platform and Section 6 concludes with the main findings of this research.

2. Related Works

Despite the numerous ongoing research projects by other researchers, the proposed PHIL testing environment proposed in this manuscript offers several unique benefits. In the testing setups detailed in papers [10,11], experiments are conducted at the component level, providing complete control over power-switching devices using specific control schemes. Conversely, our inverter is a commercially available product that is equipped with high-level smart functions such as Volt–VAR and Volt–Watt modes, and, thus, the facility has been designed to conduct tests with similar constraints to those that would be present in the field where direct control on the switching devices is not possible.

In addition, for solar farms, it is crucial to consider certain safety measures to maintain grid stability [12]. Specifically, solar farms must prioritize grid stability before scaling up the implementation of the smart functions, such as the ones implemented in commercial inverters. We take full advantage of the smart inverter functions available in our PHIL testbed to further study the impact of smart functionalities. In references [8,13,14], the authors implemented a similar approach to establish their testing setup. In contrast, our testing environment is seamlessly integrated with a Distributed Energy Resources Management System (DERMS) developed by Smart Grid Solutions. This particular system is currently undergoing deployment across multiple solar farms.

Finally, our testing facility takes advantage of the capability of examining how inverters interface with the grid while improving the DERMS functions. This capability holds significant importance for distribution system operators as it helps address challenges posed by Distributed Energy Resources (DERs) and enables the optimization of renewable energy resource benefits [15].

3. PHIL Laboratory Experimental Facility

The primary objective of the facility is to exert full control over the input and output voltages and currents of the smart inverter while operating in various modes, including Volt–VAR, Volt–Watt, and fixed power factor. Figure 1 depicts the electrical design schematic of the overall laboratory setup at ALSET Lab, Rensselaer Polytechnic Institute, along with the model numbers and brief descriptions of each component, which are listed in Table 1. In Figure 1, the power flow in the lab setup starts from the "Power Inverter" (blue dashed square), to the "Transformer" (green dashed square), and to the grid emulation (red dashed square) sub-systems. To keep the design within budget, the main design constraint was the

capacity of the power amplifier that could be purchased. This led to the choice of a 15 kW bi-directional power amplifier, the OP1400, comprising two key devices labeled with 3 and 4 in Figure 1.

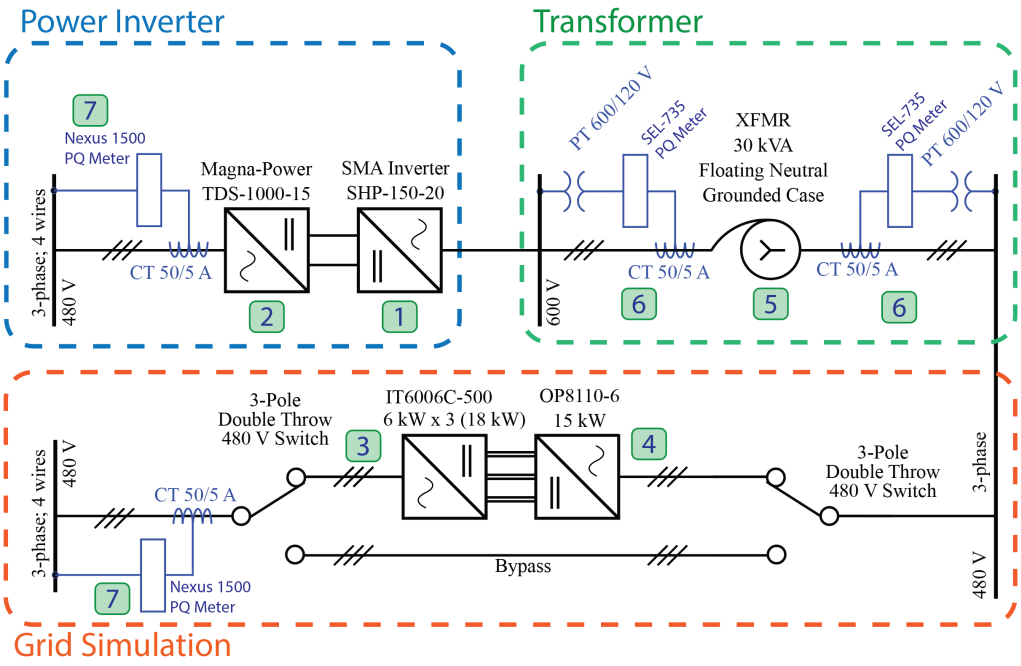

Figure 1. Overall PHIL lab design schematic.

Table 1. Table of main test-bench equipment.

Label	Equipment	Description
1	SMA SHP-150-20	SMA Inverter
2	TDS-1000-15	PV Emulator
3	IT6006C-500	Power Amp. DC Power
4	OP8110-6 and -3	Power Amplifiers
5	AUT-MIT-114	Grid Transformer
6	SEL-735	PQ Meter
7	Nexus 1500	PQ Meter

The result of this choice determined all subsequent choices for other equipment and the result is that the current test specimen, SMA's SHP-150-20 smart inverter, can only be tested at 12% of its nameplate capacity. Although this choice did not impact the ability to carry out tests, it does imply that the tests would be conducted at a maximum of 10% of the inverter's nameplate capacity.

3.1. OP1400 Power Amplifier

In [16], a switching converter is implemented as a power amplifier for evaluating the Hardware Under Test (HUT). This publication introduces a novel method for bridging the gap between simulation and the actual HUT in real-world scenarios. These features are integrated with the OP1400 PHIL Test Bench shown in Figure 2. The test bench consists of the OP8110 (a 4Q power amplifier) and the IT6006C-500 (a bi-directional power supply). Further details on these components are provided in the respective figures and additional information can be found at the provided link. (See https://tinyurl.com/OP1400 (accessed on 1 December 2023) for detailed information.)

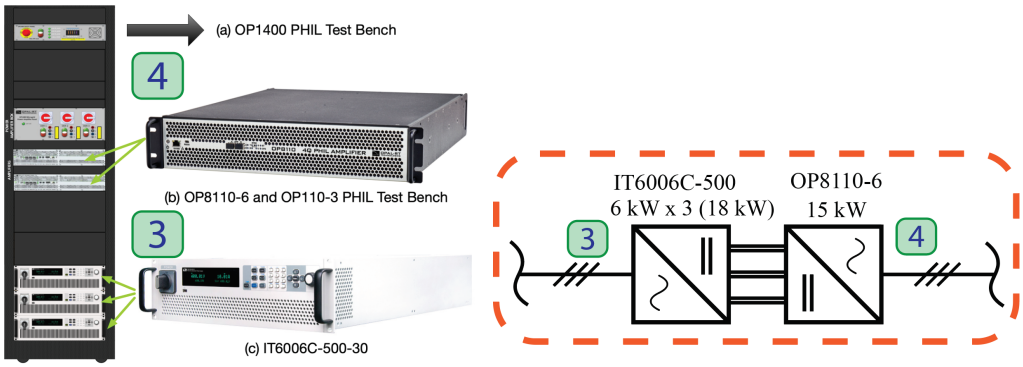

Figure 2. OP1400 PHIL test bench.

3.1.1. OP8110 4-Quadrant Power Amplifier

The OP8100 4-quadrant power amplifier as implemented in Figure 2 is capable of absorbing/injecting 15 kVA of power. This amplifier acts as a power grid emulator for the PV inverter it is connected to. As a 4-quadrant amplifier, it can absorb power from the inverter being tested. It produces a controlled 277/480 Vrms 3-phase voltage during its operation to emulate standard grid conditions. The amplifier's output voltage and frequency are adjustable, allowing us to perform low/high-frequency ride through and low/high-voltage ride through tests on the inverter. We control these tests using a real-time simulator (OP5031 and OP4520).

3.1.2. IT6006C-500 Power Supply

The OP1400 test benches, illustrated in Figure 2a, are equipped with three ITECH IT6000C series bi-directional DC power supplies, as seen in Figure 2c. These power supplies provide a stable 500V DC input voltage to the OP8110 4-quadrant amplifiers, facilitating their ability to inject or absorb power from/to the 3-phase input.

3.2. DC Power Supply

To supply DC voltage/current to the smart inverter and emulate photovoltaic (PV) array behavior, using a DC power supply is a common approach in equipment testing. The Newton–Raphson Method, presented in articles [17,18], effectively replicates the power curve of a PV panel. The approach in [17] is particularly noted for its faster settling time compared to programmable power supplies. However, in our specific testbed application, the required power rating exceeds our lab's capabilities. Consequently, we use the Magna-Power programmable DC power supply, depicted in Figure 3a, which offers programmable voltage, current, protection settings, and high-accuracy measurements. This power supply employs high-frequency IGBT-based power processing in a current-fed topology for improved control and system protection, contrasting with the conventional voltage-fed topology. This topology adds an extra stage, safeguarding the power supply even under fault conditions by preventing rapid current spikes and magnetic core saturation. The Photovoltaic Power Profile Emulation (PPPE) software 2.0.0.12, illustrated in Figure 3b, automatically generates solar array voltage and current profiles based on set parameters. These profiles are sequentially fed to the Magna-Power supply for emulation. The software enables the creation and sequencing of numerous profiles over time, facilitating controlled, repeatable experiments to assess the inverter's performance.

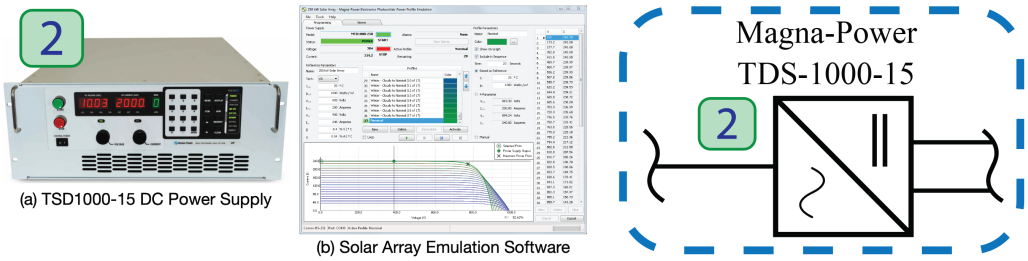

Figure 3. TSD1000-15 DC Power Supply.

3.3. SMA Inverter

In our experimental setup, the SMA SHP 150-US-20 inverter shown in Figure 4 is the primary Hardware Under Test (HUT). A notable feature of this SMA inverter is its capability to operate in various control modes, adapting to the grid operator's specific needs. For example, in fixed power mode, the inverter maintains a steady power output regardless of changes in irradiance or temperature. In Volt–VAR mode, it modulates voltage and reactive power to keep a certain power factor at the grid connection point. In frequency–watt mode, the inverter adjusts its active power output to keep the grid frequency within a specified range. By evaluating the inverter's performance across these different modes, we can verify its effectiveness and efficiency under diverse real-world conditions.

Figure 4. SMA SHP-150-20 Inverter.

3.4. PQ Meters

To ensure precise measurements in our experiments, we incorporate two types of Power Quality (PQ) meters: the Nexus 1500+ and the SEL-735 (Figure 5). These meters are strategically positioned within our system, as indicated in the schematic diagram, shown as device number 6 and 7 in Figure 1 . This placement enables us to accurately capture key parameters such as voltage, current, real power, reactive power, and other important measurements.

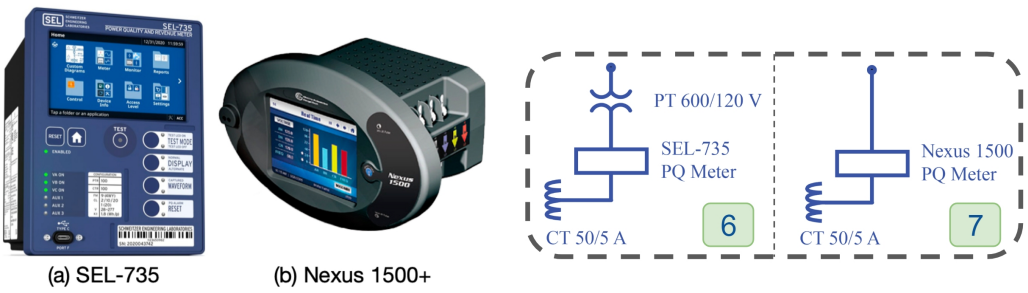

Figure 5. SEL-735 and Nexus 1500+ Meters.

3.5. Autotransformer

The autotransformer shown as device number 5 in Figure 1 in our experimental setup is essential for meeting the required specifications. As previously noted, the power amplifier

that simulates grid behavior has a voltage limit of up to 240 V L-N, considerably less than the inverter's rating of 346V L-N. To reconcile this discrepancy, we have included a 30 kVA Maddox three-phase dry-type autotransformer within the system. This autotransformer steps up the output of the amplifier to align with the inverter's higher voltage rating.

3.6. ANM Strata System

The Strata Grid system implemented in this project consists of a Core machine operating on a Linux Server, a Comms Hub machine functioning on a Windows server, and an Element Grid, also known as the ANM Element, running on an SEL RTAC 3505-5 device. Illustrative of this configuration, Figure 6 in the report presents the Strata Grid server rack, a photograph captured within the RPI Laboratory. In this image, the Element Grid RTAC is discernible as a slender blue box, while the Core and Comms Hub machines are represented by the larger two boxes.

Figure 6. Strata Grid system in RPI Lab.

Further detailing the system's structure, Figure 7 offers a comprehensive view of the system architecture, encompassing the various communication protocols each element utilizes. Of particular note within the context of the subsequent tests detailed in this report is the connection between the ANM Element and the SMA Inverter, which is facilitated through Modbus communication. This crucial link enables the transmission of commands from the Strata Grid User Interface to the SMA Inverter, a process central to the execution of numerous tests discussed in the report.

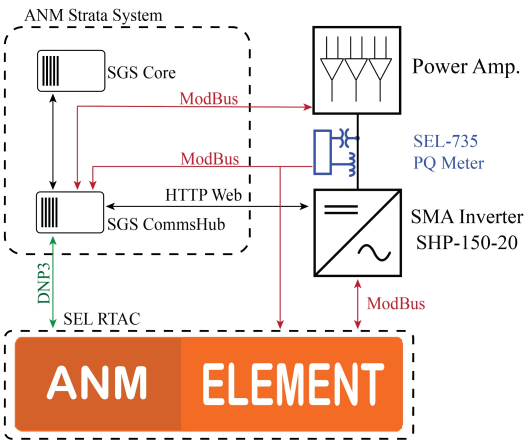

Figure 7. ANM Strata system architecture.

Additionally, the connection between the ANM Element and the SEL-735 Meter, also utilizing Modbus for communication, is another critical aspect of the system. This connection is the primary source for the real-time measurements displayed on the custom dashboard, as depicted in Figure 8. This intricate network of connections and communications forms the backbone of the Strata Grid system, enabling the advanced functionalities and tests explored in this research.

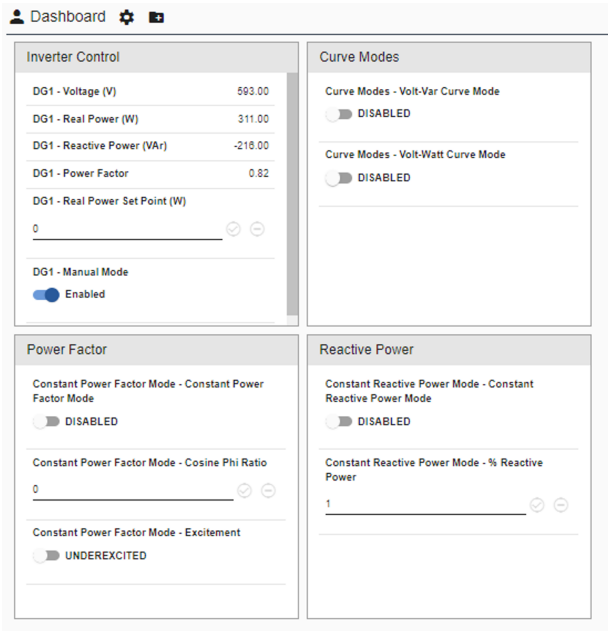

Figure 8. Strata Grid UI dashboard.

4. System Integration and Experiment Automation

4.1. System Integration

In this section, we provide an overview of the sophisticated equipment integrated into our experimental setup. This comprehensive integration of equipment is designed to create a robust and accurate testing environment, allowing for detailed analysis and evaluation of the inverter's performance under various conditions.

4.1.1. DC Power Supply

In Figure 9, the rear view of the power supply reveals key components: a current transformer (indicated by a green arrow) is used for measuring the input 480 V current, and the output terminals for Positive and Negative (marked by a blue arrow) DC power provide the input for the inverter. The RS-232 serial input, marked by a red arrow, connects the solar panel emulation software on the host computer. Similarly, the Ethernet port, indicated by a yellow arrow, is connected to the central switch. This setup allows for remote control of the DC power supply, offering flexibility in operation through both the serial port and the Ethernet interface.

Figure 9. TDS-1000-15 DC power supply instrumentation and communications wiring. Blue Arrow: Output of DC power supply. Yellow Arrow: Ethernet Connection. Red Arrow: RS-232 Connection.

4.1.2. Inverter

Figure 4 showcases the connections required to integrate the inverter into our setup. The red arrow identifies the DC power input to the inverter, which plays a crucial role in converting DC power from solar panels to AC power. The blue arrow points to the inverter's output, which supplies AC power to the load. The green arrows highlight the connections to the potential transformer and current transformer, which are essential for the SEL-735 Power Quality (PQ) meter. Lastly, the yellow arrow marks the Ethernet port, linked to the central switch via an Ethernet cable. This setup enables communication with the SGS Strata Distributed Energy Resource Management Software (DERMS) platform using the ModBus protocol, facilitating remote control and monitoring of the system.

4.1.3. Transformer

As shown in Figure 10, our experimental setup has the capability to bypass the inverter and connect directly to the power grid. In such scenarios, the autotransformer should be configured with 480Y (H4 H5 H6) on the low side for grid connection. In this configuration, the inverter is connected to a 480V grid bypassing the power amplifier. The autotransformer needs to step down the voltage from 600 V to 480 V. Operating in this mode enables the verification of both the inverter's configuration and the Distributed Energy Resource Management (DERM) system setup independently, without the necessity for the power amplifier to emulate the grid voltage. This direct connection method allows for an initial systems check before full-scale testing with a power-amplifier-based grid simulation. Conversely, when using the power amplifier to emulate the grid, it is connected to 240Y (X4 X5 X6), as detailed in Table 2. It is crucial to manually verify the status of these connections before energizing the system to ensure safety and proper functioning.

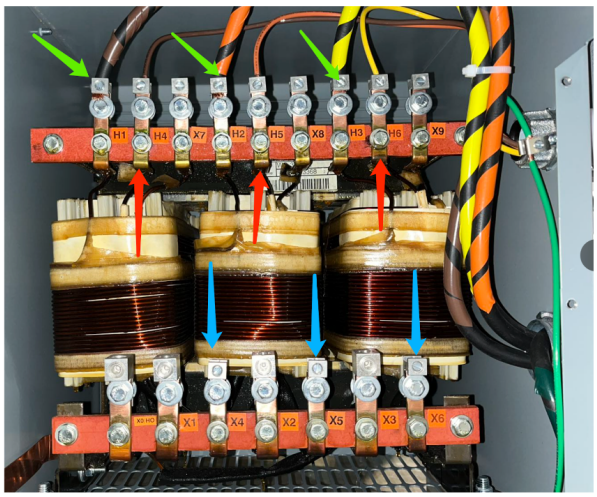

Figure 10. Autotransformer wiring. Green Arrow: Highside. Blue Arrow: Lowside

Table 2. Transformer specifications.

Voltage	Current	Connection per Phase
600Y/346V	28.9	H0 H1 H2 H3
480Y/277V	36.1	H0 H4 H5 H6
400Y/231V	43.3	X0 X7 X8 X9
240Y/139V	72.2	X0 X4 X5 X6
208Y/120V	83.3	X0 X1 X2 X3

4.1.4. Power Amplifier Wiring

In Figure 11A, the three-pole double-throw switch on the right, connected to the front panel of the OP1400 test bench, plays a crucial role. When this switch is in the

closed position (upward, as indicated by the blue arrow), the test bench is connected to the autotransformer. In Figure 11B,C, the red arrow points to the location of the banana plug. This design allows for easy alteration of the wiring configuration and voltage verification using a multimeter. The banana cables are used to connect the power amplifier to the autotransformer. In our setup, to optimize the power amplifier's performance, it is configured in differential mode, as shown in Figure 11D. Since the inverter lacks a neutral connection, both the amplifier and the inverter are wired using a floating neutral scheme to ensure proper operation.

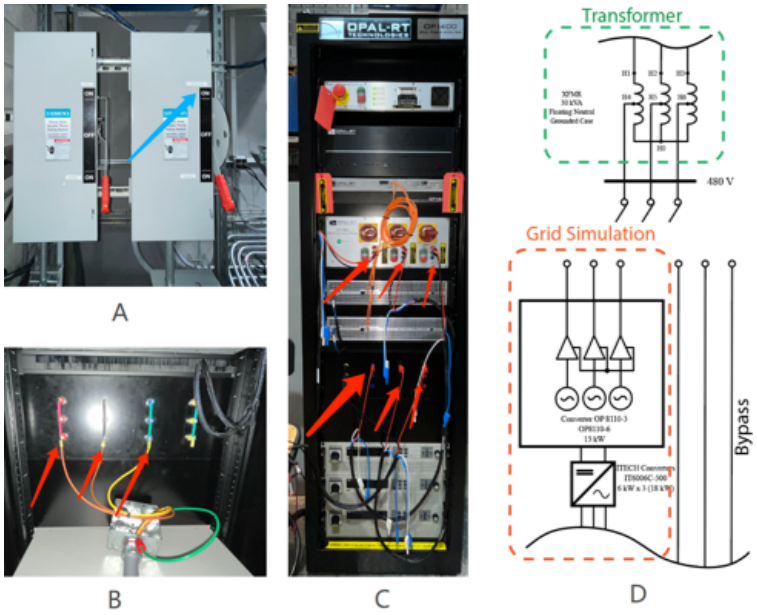

Figure 11. OP1400 Power Amplifier Wiring.

4.2. DERM System Integration

The dashboard presented in Figure 8 features several key components. In the top left corner, metrics are displayed, sourced from the SEL-735 Meter via Modbus. This same panel also allows for the input of a real power setpoint in Watts. In the upper right panel, there are toggle switches for activating Volt–Watt and Volt–VAR curves. While these curve values are currently configured in the SMA inverter's user interface, future versions of this project could integrate them directly into the dashboard. The bottom left panel is dedicated to the Constant Power Factor Mode, offering configuration parameters. This includes a toggle switch for enabling the mode and options to set the inverter to underexcited or overexcited (lagging or leading, respectively). An input box is provided for setting the desired power factor (cosine phi ratio) that the system will maintain. Finally, the bottom right corner houses the Constant Reactive Power Mode panel. This features an enable switch and an input box for specifying the desired reactive power value, expressed as a percentage of Pmax. These panels offer comprehensive control and monitoring capabilities for the system, enhancing its versatility and ease of managing DERs.

Beyond these tests, which are addressed in the custom dashboard, there are also functionalities covered out of the box with the Strata Grid UI. The first, as seen in Figure 12 is the DER Monitoring and Control. With this page, the user can see key metrics for the SMA inverter as well as perform actions such as putting the device In and Out of Service.

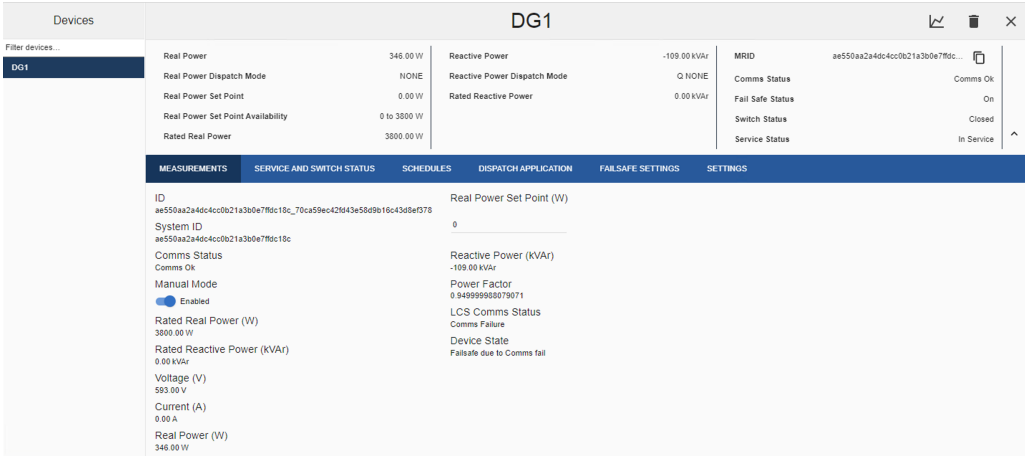

Figure 12. DER Monitoring and Control.

Another key functionality covered out of the box by Strata Grid UI is the ability to set dispatch schedules for the SMA Inverter. As seen in Figure 13, the user can configure schedules with a high level of customizability.

Figure 13. Distributed Energy Resource Management (DERM) Control User Interface (UI), displaying the feature to set the desired dispatch schedule provided by Strata Grid.

4.3. Networking and Communication

Figure 14 summarizes the communication structure of our inverter test-bench setup. The network is divided into two separate regions: local TCP/IP network and remote network. On the remote network, we can access the SGS strata and Host PC(s) remotely over the Internet with remote software like Jump-Desktop (Ver. 8.6.6), TeamViewer (Ver. 15.51.6), etc. The orange bus stands for ModBus protocol. The blue dashed bus indicates that an RS232 connection is used to control the DC power supply with PV emulation software. Modbus has emerged as a standard communication protocol, widely adopted for industrial electronic devices. It is particularly esteemed for its simplicity, ease of deployment, and open-source availability, making it an ideal choice for facilitating interoperability among various components within the smart grid infrastructure. In our experimental setup, the Modbus protocol is utilized to establish a seamless and real-time exchange of data and control commands between the smart inverter and the DERMS. This protocol supports the transmission of operational parameters, status updates, and control signals over a single network, ensuring that the inverter operates in harmony with grid conditions and management strategies. By leveraging the Modbus protocol, our research aims to demonstrate the feasibility and effectiveness of integrating advanced inverter functionalities with DERMS, highlighting the protocol's critical role in enhancing grid stability and efficiency through improved communication and control capabilities.

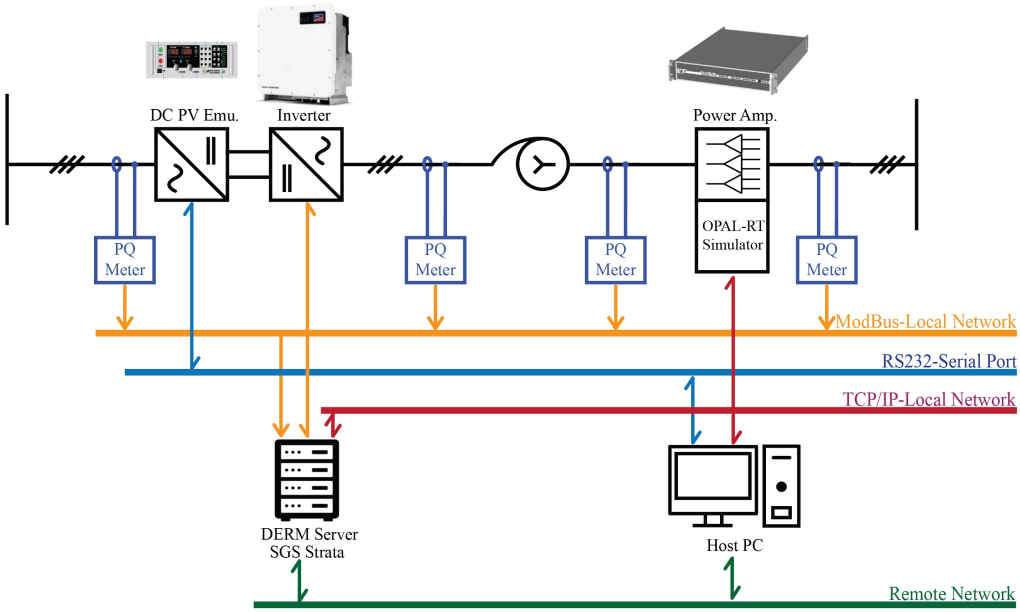

Figure 14. Communications networking.

All the devices are connected to a central switch via Ethernet cables as shown in Figure 15. With the pf-sense software installed on the server, we can easily manage the device's IP and MAC addresses.

Figure 15. Network switch.

5. Experimental Results

The test conditions used in the following test are illustrated in Table 3. All the measurements in the following tests are taken when the system reaches steady states. Therefore, although the power factor settings may differ across various tests to simulate different grid scenarios, the conditions outlined in Table 3 represent the baseline parameters. These include the voltage range, frequency, and other pertinent settings that are standard across all tests unless otherwise specified.

Table 3. Transformer specifications.

DC PV Emulation Side		Inverter AC Grid Side	
V_{MPP}	800 V	Phase Num.	3
I_{MPP}	4.5 A	$V_{RMS\ P-P}$	600 V
V_{OC}	1000 V	Nominal Frequency	60 Hz
I_{SC}	4.5 A	Max Power Per Phase	±5 kVA

5.1. Constant Power Factor Mode

It is essential to comprehend how an inverter interacts with the grid when operating under constant power factor conditions, particularly for the successful integration of renewable energy sources. This is because such interactions can influence grid stability and efficiency [19,20]. In our upcoming test, we will explore the inverter's constant power factor (pf) mode, setting it to a 0.95 lagging power factor. This setting is adjusted using the DERM user interface discussed in Figure 8. We plan to collect measurement data once the inverter has completed its power output adjustments and reached a steady state. The aim of these recordings is to confirm whether the inverter consistently maintains the desired active and reactive power levels.

Figure 16 displays the inverter producing 3 kW of power with a power factor of 0.95, aligning with expectations. Given that the SMA inverter has a capacity of generating up to 150 kW, an error margin of 158 W is considered to be within acceptable limits.

	A	B	C
I MAG (A)	2.79	2.81	2.86
	AB	BC	CA
V MAG (V)	603.98	601.38	600.85
	3P		
W (W)	2747.32		
U (VA)	2916.09		
Q (VAR)	977.66		
TRUE PF	0.94		
	LAG		
FREQ (Hz)	60.00		

Figure 16. SEL-735 meter measurements under 0.95 lagging power factor.

From the oscilloscope measurements shown in Figure 17, we found a time lag of 827 microseconds, which translates to an angle of approximately $\hat{\phi} = 17.8^{o}$. The target angle for this setup is $\hat{\phi} = 18.2^{o}$. The measured lag angle is very close to the desired value. It is important to note that the waveform exhibits slight distortion, which could explain the minor discrepancy in angle measurement. This error could be due to issues with the instrumentation or the method used for estimating the angle. However, the deviation is minimal and falls within acceptable tolerance levels.

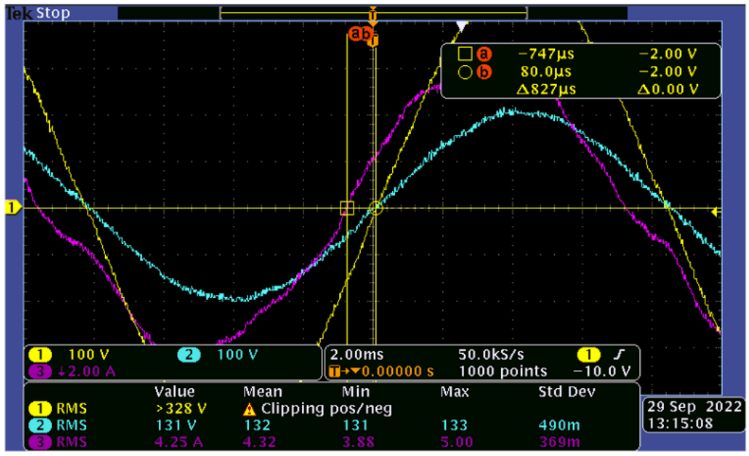

Figure 17. Yellow: transformer voltage measured at the HV side, blue: transformer voltage measured at the LV side, pink: inverter current.

We also conducted a similar test for an overexcited (leading) power factor of 0.95 measured by the PQ meter (6) on the inverter side shown in Figure 1. The results of this test are detailed in Table 4 and they show a level of accuracy comparable to that of the previous test with an oscilloscope.

Table 4. 0.95 Leading constant power factor test results.

Power	Desired	Measured	Error
Real	3000 W	2747 W	8.4%
Apparent	3162 VA	2916 VA	7.8%
Reactive	986 Var	977 Var	0.9%
P.f.	0.95	0.94	1%

5.2. Constant Reactive Power Mode

Inverters in constant reactive power mode are important in supporting grid voltage stability, especially in systems with variable loads. This mode allows inverters to either absorb or supply reactive power as needed, contributing to the maintenance of voltage stability. The utility of the constant reactive power control mode has been explored in various studies. For instance, one paper [21] delved into this control method, while another study, [22], "investigated its implementation in Norway's Vestfold and Telemark regions". These investigations pave the way for practical applications, demonstrating how the constant reactive power mode can be effectively utilized in real-world settings.

Our upcoming test will evaluate the constant reactive power mode of the inverter. As outlined in the user interface described in Figure 8, the inverter is set to maintain a constant reactive power of 750 VAR, with real power fixed at 3 kW. Figure 18 presents a selection of measurement samples from the experiment and we organized the data into a Table 5. These measurements will help us ascertain whether the inverter consistently outputs and maintains the set reactive power.

	A	B	C
I MAG (A)	2.75	2.77	2.82
	AB	BC	CA
V MAG (V)	603.40	600.80	600.45
	3P		
W (W)	2769.26		
U (VA)	2879.55		
Q (VAR)	789.33		
TRUE PF	0.96		
	LAG		
FREQ (Hz)	60.00		

Figure 18. SEL-735 meter measurements under constant reactive power mode.

Table 5. The 750 VAR constant reactive power test results.

Power	Desired	Measured	Error
Real	3000 W	2769 W	7.7%
Apparent	3092 VA	2879 VA	6.9%
Reactive	−750 Var	789 Var	5.2%

5.3. Volt–VAR Mode

Inverters equipped with Volt–VAR mode play a critical role in grid stability by adjusting their reactive power output in response to voltage fluctuations. This capability is especially beneficial in managing voltage levels in distribution networks that experience significant variations in load or generation [23]. Such dynamic voltage regulation, which traditionally relied on devices like capacitor banks, is now increasingly facilitated through the use of smart inverters. These advanced inverters offer new possibilities for sophisticated voltage management scenarios, enhancing the overall stability and efficiency of the power grid [23].

In this test, the Volt–VAR functionality of the inverter is tested. Utilizing the DERM user interface, as detailed in Figure 8, the active power of the inverter is set to remain constant. The anticipated reactive power output for this test is depicted in Figure 19. The target three-phase voltage is programmed to fluctuate within the range of 560 V to 640 V RMS, at a rate of less than 0.2 V/s. This setting is designed to assess the inverter's response to these voltage variations. The resulting Volt–VAR curve, reflecting the inverter's performance under these conditions, is presented in Figure 19. The curve is derived from data obtained from the meter during the test.

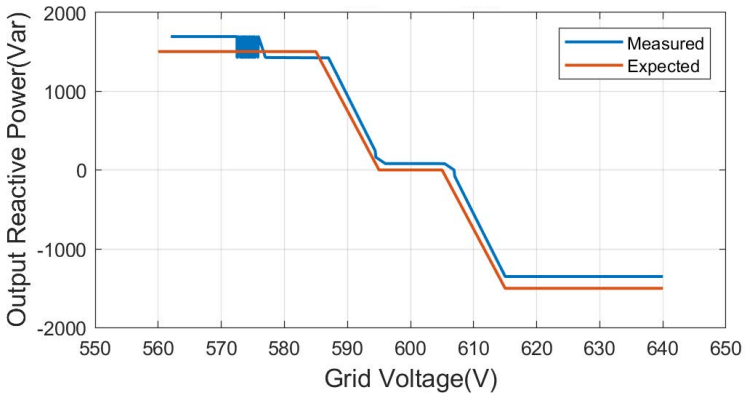

Figure 19. Measured and expected Volt–VAR curve.

The performance of the Volt–VAR mode, as shown in Figure 19, aligns with our expectations. We observe a close match between the measured Volt–VAR characteristic curve (displayed in blue) and the predefined curve within the inverter (shown in red).

An important aspect to note is that the reactive power becomes nonzero when the voltage varies between 595 V and 600 V. This measurement is recorded at the inverter's terminal while the transformer is energized.

Another noteworthy observation is the oscillations in reactive power output when the voltage fluctuates between 570 V and 590 V. The main challenge faced during our experiments is when the reactive power is relatively high (for its dispatch condition) the MPPT (maximum power point tracking) algorithm will adversely interact with the DC power supply that is conducting PV emulation. When the interaction occurs the operating point will vary within the blue circle shown in Figure 20, akin to an oscillation.

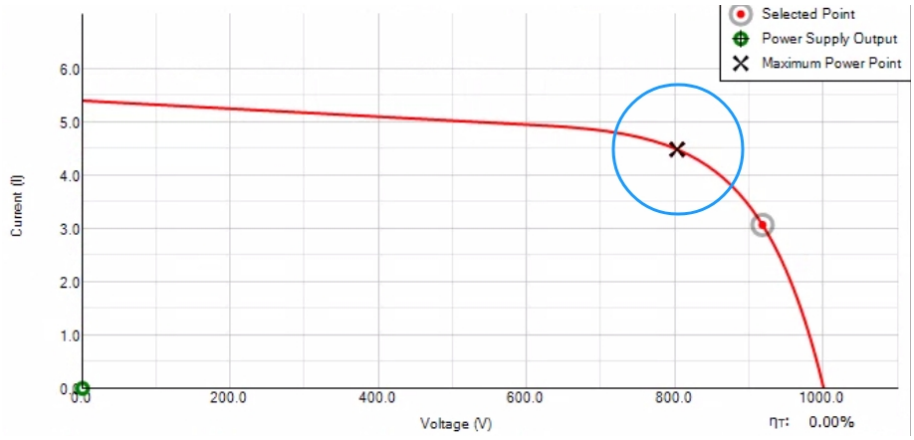

Figure 20. Oscillation range shown on the PV emulation IV curve.

Theoretically, the operating point should always stay on the red IV curve. When emulating a PV panel the DC power supply control mode switches between a (CC) current-controlled source and a (VC) voltage-controlled source to keep the operating point on the curve [18]. Thus we suspect that the observed interaction is a result from the PV emulation software switching between CC and VC modes, the tuning of the internal current or voltage loops, and the MPPT algorithm of the inverter trying to find the maximum power point.

There are two approaches to address this issue, one based on hardware and one based on software. A potential hardware-based solution would be to add a capacitor at the output of the DC power supply to offset the resonant frequency that results from the control mode switching. However, we have not yet conducted the experimental validation to verify whether adding a capacitor at the output will resolve this issue. The proposed solution is based on our preliminary analysis and theoretical understanding of the system dynamics. A potential software-based solution would be to change the behavior of the PV emulation software; however, this is not possible as the authors do not have access to the source code. Hence, a software-based approach would imply the development of a software suite to perform PV emulation and control the DC supply, which is an effort outside the authors' work scope and possibilities. Therefore, future work will involve setting up a series of controlled experiments to test the efficacy of the hardware-based solution (i.e., additional DC output capacitor) under various operating conditions. Future work will attempt to model this interaction and analyze potential solutions to avoid this issue during testing, such as a new testing procedure or additional equipment to install on the DC side.

5.4. Volt–Watt Mode

The Volt–Watt mode is particularly crucial in contexts with a high presence of photovoltaic (PV) systems. Excessive solar generation can lead to over-voltage problems in the electrical grid. Inverters with Volt–Watt functionality can mitigate these risks by decreasing their power output as the grid voltage rises, thus helping to prevent over-voltage issues [24,25]. Our subsequent test demonstrates the operational characteristics of this mode under controlled conditions. The comparison between the measured and expected Volt–Watt curves is depicted in Figure 21, with data sourced from the power meter.

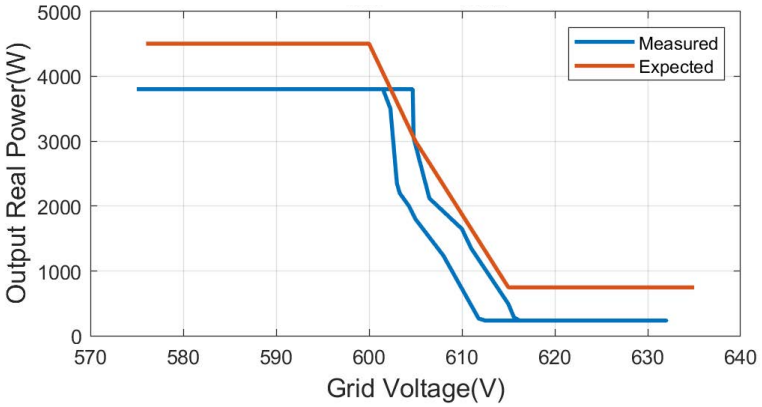

Figure 21. Measured and expected Volt–Watt curve.

The test results illustrated in Figure 21 indicate that the Volt–Watt mode's overall performance generally meets our expectations. However, a key observation from the comparison of the measured Volt–Watt curve (shown in blue) with the desired curve (illustrated in red) is that the output power is considerably lower than expected. It is important to note that these tests utilize only a small portion of the inverter's full 150 kW capacity. Our current theory is that the inverter's control system may allow for a certain degree of error margin.

Additionally, the presence of hysteresis in the Volt–Watt retained curve is unexpected and needs further investigation. Understanding the reasons behind this hysteresis is crucial for optimizing the inverter's performance in Volt–Watt mode. Further studies are necessary to explore and clarify the underlying causes of this phenomenon.

5.5. High/Low-Voltage Ride Through

Voltage ride through (VRT) plays a critical role in sustaining grid stability amidst transient voltage disturbances. This capability allows inverters to keep functioning and support the grid during brief instances of under- or over-voltage, which is frequently implemented in power systems [26,27]. The importance of VRT lies in its ability to ensure the continuous operation of inverters, thereby contributing to the overall reliability and resilience of the electrical grid.

For this test, the lower maximum voltage threshold is set at 640 V with a 20 s tripping time. If the voltage exceeds 640 V for a duration shorter than 20 s, the inverter should not trip. Similarly, the upper minimum voltage threshold is established at 500 V with the same 20 s tripping time. In this case, if the voltage falls below 500 V for less than 20 s, the inverter is expected to maintain its operation and the opposite scenario should result in a trip. This test aims to assess the inverter's ability to withstand short periods of voltage fluctuations.

In Figure 22, the voltage dropped below 500 V at 760.76 s. Subsequently, the inverter's output power fell to zero at 780 s, which aligns with our expectations considering the tripping time was set to 20 s. Additionally, at 962.92 s, there was another instance where the voltage dipped below 500 V but this time for 8 s. In this case, the inverter successfully maintained its power output at the preset level, demonstrating its effective response to transient voltage disturbances within the specified tripping time parameters.

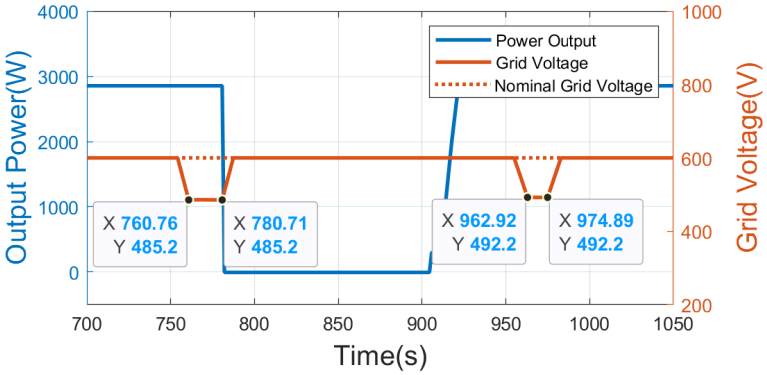

Figure 22. Low- voltage ride through test.

In Figure 23, the inverter tripped at 780 s because the grid voltage exceeded 640 V for a period longer than the established 20-second tripping time. Conversely, when the grid voltage was above 640 V but for a duration shorter than 20 s, the inverter successfully maintained its output power at 3 kW. This behavior illustrates the inverter's adherence to the set tripping time criteria in voltage ride through (VRT) scenarios, effectively handling both prolonged and brief over-voltage conditions.

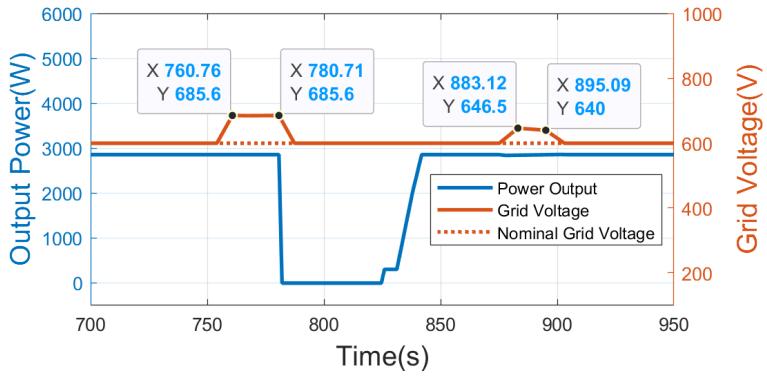

Figure 23. High- voltage ride through test.

5.6. Return-to-Service Test

Following events like faults in the grid or power outages, the prompt reactivation of inverters plays a crucial role in sustaining the supply to local loads. The "Return to Service Wait" period is a critical interval that utilities can use to specify a time for inverter reconnection. Setting this period helps ensure that inverters reconnect to the grid only when stable conditions are re-established, as recommended in relevant standards such as the IEEE standard [28]. This practice is vital for maintaining grid stability and safety during the recovery phase after disruptions.

In this test, the active power for this test is preset to 3 kW and the reconnection time after experiencing a grid fault is set at 2 min. The expectation is that the inverter will resume normal operation and come back online within 2 min after it detects a stable grid voltage, specifically around 600 V. This test aims to verify the inverter's compliance with the set reconnection time and its ability to effectively re-engage with the grid under normal voltage conditions.

In Figure 24, the inverter registers a nominal voltage at 782.04 s and commences increasing its output power at 904.4 s. The duration of the wait before the inverter starts ramping up is 122.36 s, closely aligning with the anticipated reconnection time of 120 s. This observation confirms the effective operation of the inverter's return-to-service function, demonstrating its ability to re-engage with the grid after a disturbance.

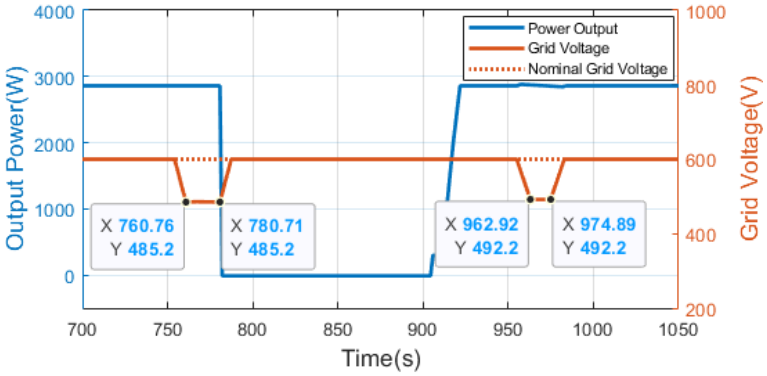

Figure 24. Return- to-service test.

5.7. Output Power Deviation Analysis

To address the uncertainty in the output power of the inverter, we present the accompanying histogram in Figure 25, which illustrates the distribution of the inverter's power output deviations from the expected value. This histogram is constructed by normalizing the data—each measurement is adjusted by subtracting the dataset's mean value, centering the distribution around zero. These measurements were taken from the experimental conditions detailed in Table 3, where the inverter's target output was set to 3 kW at a unity power factor. A total of 510 data points were collected over 35 s, providing a dataset for analysis. The calculated variance of the power output is 3.8 W, which offers insight into the spread of the data. The mean output power is determined to be 2851 W, with a standard deviation of approximately 1.95 W, quantifying the inverter's average deviation from the expected output. This standard deviation represents the inverter's precision and, alongside the average value, serves as a metric for characterizing the error to the expected response. The close clustering of data points around the mean value, as observed in the histogram in Figure 25, reaffirms the inverter's generally consistent performance within the expected operational range.

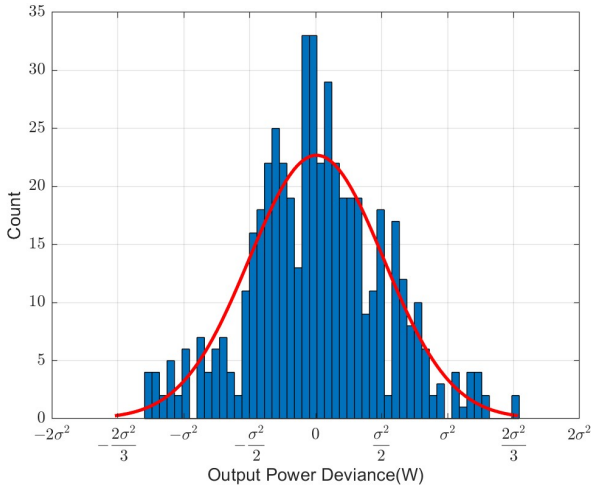

Figure 25. Distribution of output power deviance for inverter.

6. Conclusions

The Power Hardware-in-the-Loop (PHIL) experimental facility at Rensselaer Polytechnic Institute has been effectively utilized to evaluate the performance of an inverter under various operating conditions and control modes with a DERMS system.

This work developed and applied a suite of comprehensive test protocols to evaluate the performance of smart inverters in real time and under real-world conditions representing a significant theoretical advancement in the area of experimental testing. Using the developed testing protocols, the following PHIL tests were conducted, each using a

different smart inverter functionality: 1. constant power factor, 2. constant reactive power, 3. Volt–VAR, 4. Volt–Watt, 5. voltage ride through, all conducted in line with the IEEE 1547.1-2020 standard. The quantitative results from the PHIL testing environment provide substantial evidence of the smart inverter's performance across various operational modes, highlighting its stability, control accuracy, and response to grid disturbances.

This work also integrated the DERMS and used it to automatically conduct the experiments that are used to verify the smart inverter functionalities. This approach, if adopted, would allow the operator of the DERMS to routinely perform tests on smart inverters in the field to verify their performance, facilitating more routine performance assessment of such devices to mitigate potential issues related to control interactions with the grid.

The findings demonstrate that the PHIL testing environment is proficient in validating the functionalities of the smart inverter with DERM system. However, it is important to acknowledge some discrepancies observed between the expected and measured outputs of the inverter. These discrepancies are primarily attributed to the non-linear behavior of the current and voltage transformers used in the instrumentation. Additionally, the experiments revealed an adverse interaction between the DC power supply and the inverter, which resulted in unforeseen variations in output power. This phenomenon warrants further investigation. To enhance the testing setup, it is recommended to modify the configuration of the amplifier, especially for experiments necessitating a higher power rating. Such adjustments will enable the more accurate and comprehensive testing of smart inverters in future studies.

Author Contributions: H.C.: Conceptualization, Data Curation, Formal Analysis, Investigation, Methodology, Software, Validation, Visualization, Writing—Original Draft. L.V.: Conceptualization, Formal Analysis, Funding Acquisition, Investigation, Methodology, Project Administration, Resources, Supervision, Validation, Writing—Original Draft, Writing—Review and Editing. All authors have read and agreed to the published version of the manuscript.

Funding: This research was funded in part by the New York State Energy Research and Development Authority (NYSERDA) under agreement number 149165, in part by the ECSE department at Rensselaer Polytechnic Institute and in part by Dominion Energy.

Acknowledgments: The authors would like to thank Yusef Orest, Stuart McMahon, and Jack Rodman from Smarter Grid Solutions for their contributions in the Strata Grid software integration and project management. The authors thank Schweitzer Engineering Laboratories for the donation of the SEL-735 meters and other auxiliary equipment and to Joseph Dengel for aiding in the lab's design and metering verification. The following students also contributed to the implementation of the laboratory facility: Prottay Adhikari, Sergio Dorado, and James Choi. This paper is dedicated to the memory of Jerry W. Dziuba, who was instrumental in the implementation of the laboratory and passed away before it was completed.

Data Availability Statement: The data presented in this study are available on request from the corresponding author. The data are not publicly available due to confidentiality and privacy concerns. Before sharing the data, they need to be thoroughly reviewed, anonymized, and cleaned to ensure that no sensitive information is inadvertently disclosed. Once this process is complete, interested parties can contact the corresponding author for access to the data.

Conflicts of Interest: The funders had no role in the design of the study; in the collection, analyses, or interpretation of data; in the writing of the manuscript; or in the decision to publish the results.

References

1. *IEEE Std 1547-2018*; IEEE Standard for Interconnection and Interoperability of Distributed Energy Resources with Associated Electric Power Systems Interfaces. IEEE: Piscataway, NJ, USA, 2018; pp. 1–138. [CrossRef]
2. International Renewable Energy Agency IRENA. *Grid Codes for Renewable Powered Systems*; International Renewable Energy Agency (IRENA): Masdar City, United Arab Emirates, 2022; ISBN 9789292605100
3. North American Reliability Corporation. *Reliability Guideline. Improvements to Interconnection Requirements for BPS-Connected Inverter-Based Resources*; North America Electric Reliability Corporation (NERC): Atlanta, GA, USA, 2019.
4. Adhikari, P.M.; Hooshyar, H.; Fitsik, R.J.; Vanfretti, L. Precision timing and communication networking experiments in a real-time power grid hardware-in-the-loop laboratory. *Sustain. Energy Grids Netw.* **2021**, *28*, 100549. [CrossRef]

5. Li, S.; Zhang, L.; Paquin, J.-N.; Bélanger, J.; Vanfretti, L. Hardware-in-the-Loop Use Cases for Synchrophasor Applications. In Proceedings of the 2019 International Conference on Smart Grid Synchronized Measurements and Analytics (SGSMA), College Station, TX, USA, 21–23 May 2019; pp. 1–8. [CrossRef]
6. Adhikari, P.M.; Vanfretti, L.; Banjac, A.; Bründlinger, R.; Ruppert, M.; Ropp, M. Analysis of transient overvoltages and Self Protection Overvoltage of PV inverters through RT-CHIL. *Electr. Power Syst. Res.* **2023**, *214*, 108826. [CrossRef]
7. Guillaud, X.; Faruque, M.O.; Teninge, A.; Hariri, A.H.; Vanfretti, L.; Paolone, M.; Dinavahi, V.; Mitra, P.; Lauss, G.; Dufour, C.; et al. Applications of Real-Time Simulation Technologies in Power and Energy Systems. *IEEE Power Energy Technol. Syst. J.* **2015**, *2*, 103–115. [CrossRef]
8. Hoke, A.; Chakraborty, S.; Basso, T. A power hardware-in-the-loop framework for advanced grid-interactive inverter testing. In Proceedings of the 2015 IEEE Power & Energy Society Innovative Smart Grid Technologies Conference (ISGT), Washington, DC, USA, 18–20 February 2015; pp. 1–5. [CrossRef]
9. Pokharel, M.; Ho, C.N.M. Stability Analysis of Power Hardware-in-the-Loop Architecture with Solar Inverter. *IEEE Trans. Ind. Electron.* **2021**, *68*, 4309–4319. [CrossRef]
10. Pokharel, M.; Ho, C.N.M. Stability study of power hardware in the loop (PHIL)simulations with a real solar inverter. In Proceedings of the IECON 2017—43rd Annual Conference of the IEEE Industrial Electronics Society, Beijing, China, 29 October–1 November 2017; pp. 2701–2706. [CrossRef]
11. Nzimako, O.; Wierckx, R. Stability and accuracy evaluation of a power hardware in the loop (PHIL) interface with a photovoltaic micro-inverter. In Proceedings of the IECON 2015—41st Annual Conference of the IEEE Industrial Electronics Society, Yokohama, Japan, 9–12 November 2015; pp. 5285–5291. [CrossRef]
12. Amanipoor, A.; Golsorkhi, M.S. Stability Analysis and Design of Volt-VAR Controller for Grid Connected PV Systems with Consideration of the Impact of Voltage Feedforward. In Proceedings of the IECON 2022—48th Annual Conference of the IEEE Industrial Electronics Society, Brussels, Belgium, 17–20 October 2022; pp. 1–6. [CrossRef]
13. Mather, B.A.; Kromer, M.A.; Casey, L. Advanced photovoltaic inverter functionality verification using 500kw power hardware-in-loop (PHIL) complete system laboratory testing. In Proceedings of the 2013 IEEE PES Innovative Smart Grid Technologies Conference (ISGT), Washington, DC, USA, 24–27 February 2013; pp. 1–6. [CrossRef]
14. Crăciun, B.I.; Kerekes, T.; Séra, D.; Teodorescu, R.; Brandl, R.; Degner, T.; Geibel, D.; Hernandez, H. Grid integration of PV power based on PHIL testing using different interface algorithms. In Proceedings of the IECON 2013—39th Annual Conference of the IEEE Industrial Electronics Society, Vienna, Austria, 10–13 November 2013; pp. 5380–5385. [CrossRef]
15. Strezoski, L.; Padullaparti, H.; Ding, F.; Baggu, M. Integration of Utility Distributed Energy Resource Management System and Aggregators for Evolving Distribution System Operators. *J. Mod. Power Syst. Clean Energy* **2022**, *10*, 277–285. [CrossRef]
16. Jha, K.; Mishra, S.; Joshi, A. Boost-Amplifier-Based Power-Hardware-in-the-Loop Simulator. *IEEE Trans. Ind. Electron.* **2015**, *62*, 7479–7488. [CrossRef]
17. Das, C.; Mandal, K.; Roy, M. Design of PV Emulator Fed MPPT Controlled DC-DC Boost Converter for Battery Charging. In Proceedings of the 2020 IEEE First International Conference on Smart Technologies for Power, Energy and Control (STPEC), Nagpur, India, 25–26 September 2020; pp. 1–6. [CrossRef]
18. Wandhare, R.G.; Agarwal, V. A low cost, light weight and accurate photovoltaic emulator. In Proceedings of the 2011 37th IEEE Photovoltaic Specialists Conference, Seattle, WA, USA, 19–24 June 2011; pp. 1887–1892. [CrossRef]
19. Faizura Norhasmi, N.N.; Raveendran, S.K.; Ramachandaramurthy, V.K. Power Factor Control of Solar Photovoltaic Inverter as a Solution to Overvoltage. In Proceedings of the 2018 IEEE PES Asia-Pacific Power and Energy Engineering Conference, Kota Kinabalu, Malaysia, 7–10 October 2018; pp. 751–756. [CrossRef]
20. Rahimi, K.; Tbaileh, A.; Broadwater, R.; Woyak, J.; Dilek, M. Voltage regulation performance of smart inverters: Power factor versus volt-VAR control. In Proceedings of the 2017 North American Power Symposium, Morgantown, WV, USA, 17–19 September 2017; pp. 1–6. [CrossRef]
21. Bisht, R.; Subramaniam, S.; Bhattarai, R.; Kamalasadan, S. Active and reactive power control of single phase inverter with seamless transfer between grid-connected and islanded mode. In Proceedings of the 2018 IEEE Power and Energy Conference at Illinois, Champaign, IL, USA, 22–23 February 2018; pp. 1–8. [CrossRef]
22. Acosta, M.N.; Gonzalez-Longatt, F.; Andrade, M.A.; Rueda Torres, J. Optimal Reactive Power Control of Smart Inverters: Vestfold and Telemark Regional Network. In Proceedings of the 2021 IEEE Madrid PowerTech, Madrid, Spain, 28 June–2 July 2021; pp. 1–6. [CrossRef]
23. Vijayan, V.; Mohapatra, A.; Singh, S. Impact of Modes of Operation of Smart Inverters on Volt-VAR Optimization. In Proceedings of the 2019 IEEE PES Innovative Smart Grid Technologies Europe, Bucharest, Romania, 29 September–2 October 2019; pp. 1–5. [CrossRef]
24. Noh, J.; Kang, S.; Kim, J.; Park, J.W. A Study on Volt-Watt Mode of Smart Inverter to Prevent Voltage Rise with High Penetration of PV System. In Proceedings of the 2019 IEEE Power & Energy Society General Meeting, Atlanta, GA, USA, 4–8 August 2020; pp. 1–5. [CrossRef]
25. Kashani, M.G.; Mobarrez, M.; Bhattacharya, S. Smart inverter volt-watt control design in high PV penetrated distribution systems. In Proceedings of the 2017 IEEE Energy Conversion Congress and Exposition, Cincinnati, OH, USA, 1–5 October 2017; pp. 4447–4452. [CrossRef]

26. Sakimoto, K.i.; Sugimoto, K.; Shindo, Y. Low voltage ride through capability of a grid connected inverter based on the virtual synchronous generator. In Proceedings of the 2013 IEEE 10th International Conference on Power Electronics and Drive Systems, Kitakyushu, Japan, 22–25 April 2013; pp. 1066–1071. [CrossRef]
27. Choudhury, S.R.; Gupta, A.; Anand, S. Simulation of low voltage ride through scheme for inverters connected to distribution system with high R/X ratio. In Proceedings of the 2016 10th International Conference on Compatibility, Power Electronics and Power Engineering, Bydgoszcz, Poland, 29 June–1 July 2016; pp. 202–207. [CrossRef]
28. *IEEE Std 1547.1-2020*; IEEE Standard Conformance Test Procedures for Equipment Interconnecting Distributed Energy Resources with Electric Power Systems and Associated Interfaces. IEEE: Piscataway, NJ, USA, 2020; pp. 1–282. [CrossRef]